Lectures 14-15: Electrostatic Thrusters (Kaufman Ion Engines)

Electrostatic thrusters ("ion engines") are the best developed type of electric propulsion device, dating in conception to the 1950's, and having been demonstrated in space in 1964 on a suborbital flight of the SERT I spacecraft. The early history and concepts are well documented, and evolved through progressive refinements of various types of ion beam sources used in Physics laboratories, the improvements being essentially dictated by the needs for high efficiency, low mass and long life for these sources to be used in space. Of the various configurations discussed in the literature, only the electron bombardment noble gas type, plus (in Europe) the radio-frequency ionized thruster and (in Japan) the Electron Cyclotron Resonance thruster, have survived. Other interesting concepts, such as Cesium Contact thrusters and duo-plasmatron sources have been largely abandoned, and two new special devices, the Field Emission Electrostatic Propulsion (FEEP) and Ionic Liquid Ion Source (ILIS) have been added to the roster.

The electron bombardment thruster itself has evolved in the same time interval from relatively deep cylindrical shapes with uniform magnetic fields produced by external coils and with simple thermionic cathodes, to shallow geometrics using sharply nonuniform magnetic field configurations, produced by permanent magnets, and with hollow cathode plasma bridges used as cathode and neutralizer. While typical ion production cost is $400 - 600$ eV for Hg at 80% mass utilization fraction, additional work with ring-cusp thrusters has yielded for example a cost of 116 eV in Xenon at the same utilization. Such reductions make it now possible to design for efficient operation (above 80%) with environmentally acceptable noble gases at specific impulses below 3000 sec, a goal that seemed elusive a few years back. The major uncertain issues in this field seem now reduced to lifetime (measured in years of operation in orbit) and integration problems, rather than questions of cost and physical principle or major technological hurdles. Extensions to higher power (tens of kW) and higher specific impulse (to $7{,}000 - 8{,}000$ s) are now being pursued by NASA for planetary missions requiring high Δv.

Principles of Operation

Electrostatic thrusters accelerate heavy charged atoms (ions) by means of a purely electrostatic field. Magnetic fields are used only for auxiliary purposes in the ionization chamber. It is well known that electrostatic forces per unit area (or energies per unit volume) are of the order of $\frac{1}{2}\varepsilon_0 E^2$, where E is the strength of the field (V/m). Typical maximum fields, as limited by vacuum breakdown or shorting due to imperfections, are of the order of 10^6 V/m, yielding maximum force densities of roughly 5 N/m^2. This low force density is one of the major drawbacks of electrostatic engines, and can be compared to force densities of the order of 10^4 N/m^2 in self-magnetic devices such as MPD thrusters, or to the typical gas pressures of $10^6 - 10^7$ N/m^2 in chemical rockets. Simplicity and efficiency must therefore compensate for this disadvantage.

The main elements of an electrostatic thruster are summarized in the figure below. Neutral propellant is injected into an ionization chamber, which may operate on a variety of principles: electron bombardment (shown in the figure), contact ionization, radio-frequency ionization, etc. The gas contained in the chamber may only be weakly ionized in the steady state, but ions are extracted preferentially to neutrals, and so, to a first approximation, we may assume that only ions and electrons leave this chamber.

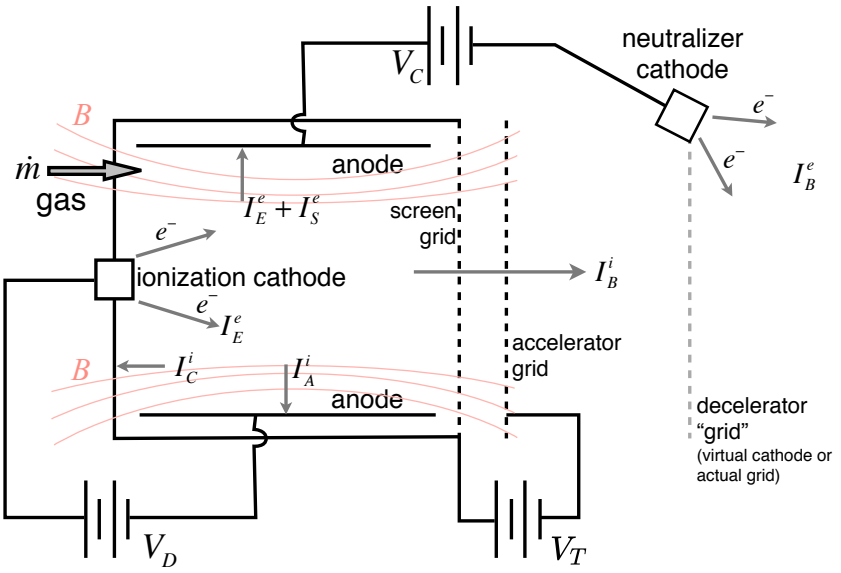

The ions are accelerated by a potential difference V_T applied between perforated plates (grids) and this same potential keeps electrons from also leaving through these grids. The electrons from the ionization chamber are collected by an anode, and in order to prevent very rapid negative charging of the spacecraft (which has very limited electrical capacity), they must be ejected to join the ions downstream of the accelerating grid. To this end, the electrons must be forced to the large negative potential of the accelerator (which also prevails in the beam), and they must then be injected into the beam by some electron-emitting device (hot filament, plasma bridge, etc).

The net effect is to generate a jet of randomly mixed (but not recombined) ions and electrons, which is electrically neutral on average, and is therefore a plasma beam. The reaction to the momentum flux of this beam constitutes the thrust of the device. Notice in the thruster figure that, when properly operating, the accelerator grid should collect no ions or electrons, and hence its power supply should consume no power, only apply a static voltage. On the other hand, the power supply connected to the neutralizer must pass an electron current equal in magnitude to the ion beam current, and must also have the full accelerating voltage across its terminals; it is therefore this power supply that consumes (ideally) all of the electrical power in the device.

In summary, the main functional elements in an ion engine are the ionization chamber, the accelerating grids, the neutralizer, and the various power supplies required. Most of the efforts towards design refinement have concentrated on the ionization chamber, which controls the losses, hence the efficiency of the device, and on the power supplies, which dominate the mass and parts count. The grids are, of course, an essential element too, and much effort has been spent to reduce their erosion by stray ions and improve its collimation and extraction capabilities. The neutralizer was at one time thought to be a critical item, but experience has shown that, with good design, no problems arise from it. Following a traditional approach, we will first discuss the ion extraction system, then turn to the chamber and other elements.

Ion Extraction and Acceleration

The geometry of the region around an aligned pair of screen and accelerator holes is shown schematically next. The electrostatic field imposed by the strongly negative accelerator

grid is seen to penetrate somewhat into the plasma through the screen grid holes. This is fortunate, in that the concavity of the plasma surface provides a focusing effect which helps reduce ion impingement on the accelerator. The result is an array of hundreds to thousands of individual ion beamlets, which are neutralized a short distance downstream, as indicated. The potential diagram shows that the screen grid is at somewhat lower potential than the plasma in the chamber.

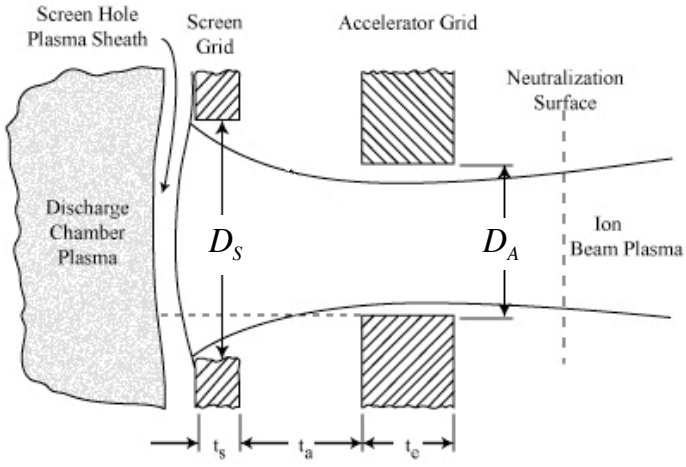

GRID GEOMETRY

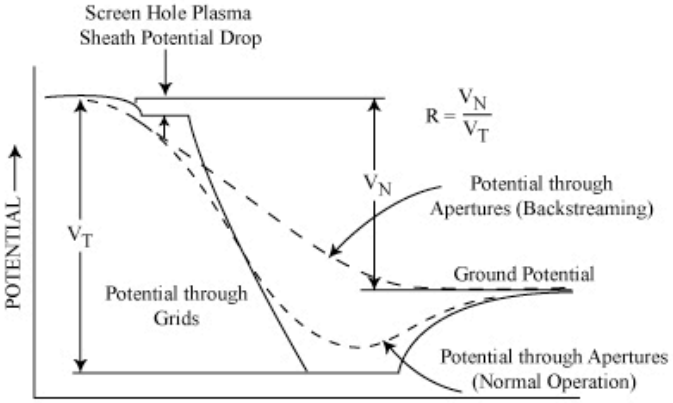

POTENTIAL VARIATION

Typically the plasma potential is near that of the anode in the chamber, while the screen is at cathode potential (some 30-60 volts lower, as we will see). This ensures that ions which wander randomly to the vicinity of the extracting grid will fall through its accelerating potential, while electrons (even those with the full energy of the cathode-anode voltage) are kept inside. The potential far downstream is essentially that of the neutralizer, if its electron-emission capacity is adequate. This potential is seen to be set above that of the accelerator grid, in order to prevent backflow of electrons from the neutralizer through the accelerating system. In addition, by making the "total voltage", V_T, larger than the "Net voltage", V_N, the ion extraction capacity of the system is increased with no change (if V_N is fixed) on the final velocity of the accelerated ions. In some designs, a third grid ("decelerator grid") is added to more closely define and control V_N, and the neutralizer is set at approximately the same potential as this third grid.

It is difficult to analyze the three-dimensional potential and flow structures just described.

It is however, easy and instructive to idealize the multiplicity of beamlets as a single effective one-dimensional beam. The result is the classical Child-Langmuir space charge limited current equation.

The elements of the derivation are outlined below:

a) Poisson's equation in the gap

$$\frac{d^2\phi}{dx^2} \;=\; -\frac{en_i}{\varepsilon_0} \tag{1}$$

b) Ion continuity

$$j \;=\; en_i v_i \;\equiv\; \text{constant} \tag{2}$$

c) Electrostatic ion free-fall

$$v_i \;=\; \sqrt{\frac{2e(-\phi)}{m_i}} \tag{3}$$

Combining these equations, we obtain a 2nd order, nonlinear differential equation for $\phi(x)$. The boundary conditions are,

$$\phi(0) = 0 \qquad \text{and} \qquad \phi(x=d) \;=\; -V_T \tag{4}$$

In addition, we also impose that the field must be zero at screen grid:

$$\left(\frac{d\phi}{dx}\right)_{x=0} \;=\; 0 \tag{5}$$

This is because (provided the ion source produces ions at a sufficient rate), a negative screen field would extract more ions, which would increase the "in transit" positive space charge in the gap. This would then reduce the assumed negative screen field, and the process would stop only when this field is driven to near zero (positive fields would choke off the ion flux). At this point, the grids are automatically extracting the highest current density possible, and are said to be "space charge limited".

Since three conditions were imposed, integration of the equations (1) to (3) will yield the voltage profile and also the current density j. The result is,

$$j \;=\; \frac{4}{9}\varepsilon_0\sqrt{2\frac{e}{m_i}}\frac{V_T^{3/2}}{d^2} \tag{6}$$

and also,

$$\phi(x) \;=\; -V_T\left(\frac{x}{d}\right)^{4/3} \tag{7}$$

$$E(x) \;=\; \frac{4}{3}\frac{V_T}{d}\left(\frac{x}{d}\right)^{1/3} \tag{8}$$

Equation (8) in particular shows that the field is zero (as imposed) at $x = 0$, and is $\frac{4}{3}\frac{V_T}{d}$ at $x = d$ (the accelerator grid). This allows us to calculate the net electrical force per unit area on the ions in the gap as the difference of the electric pressures on both faces of the "slab",

$$\frac{F}{A} \;=\; \frac{1}{2}\varepsilon_0\left(\frac{4}{3}\frac{V_T}{d}\right)^2 \;=\; \frac{8}{9}\varepsilon_0\left(\frac{V_T}{d}\right)^2 \tag{9}$$

and this must be also the rocket thrust (assuming there is no force on ions in other regions, i.e., a flat potential past the accelerator). It is interesting to obtain the same result from the classical rocket thrust equation. The mass flow rate is,

$$\dot{m} \;=\; jA\frac{m_i}{e}$$

and the ion exit velocity is,

$$c \;=\; \sqrt{\frac{2eV_T}{m_i}}$$

giving,

$$\frac{F}{A} \;=\; \frac{\dot{m}}{A}c \;=\; j\frac{m_i}{e}\sqrt{\frac{2eV_T}{m_i}}$$

Using Child-Langmuir's law for j, Eq. (6), this reduces indeed to Eq. (9).

For a given propellant (m_i) and specific impulse (c), the voltage to apply to the accelerator is fixed,

$$V_T \;=\; \frac{m_i c^2}{2e} \tag{10}$$

and, from Eq. (9), increasing the thrust density requires a reduction of the gap distance d. As noted before, this route is limited by eventual arcing or even by mechanical shorting due to grid warping or imperfections. For thruster diameters of, say, $10 - 50$ cm, gap distances have been kept above 0.5 to 1 mm.

The only other control, at this level of analysis, is offered by increasing the ion molecular mass, m_i. This allows increased voltages V_T Eq. (10), and, provided d can be kept small, higher thrust Eq. (9). In addition to increasing thrust density, higher molecular mass also reduces the importance of a given ion production cost $\Delta\phi$ (See lecture 3), and hence increases the thruster efficiency.

The effect of ion deceleration past the accelerator grid (either through the use of a "decel" grid, as seen in the figure below, or by relative elevation of the neutralizer potential) can be easily incorporated in this 1-D model. For the usual geometries, the screen-accelerator gap still controls the ion current, Eq. (6) with d replaced by d_a. This is because the mean

ion velocity is high (and hence the mean ion density is low) in the second gap, between the accelerator and the real or virtual decelerator, so that no electrostatic choking occurs there. This is schematically indicated in the figure by a break in the slope of the potential at the decelerator.

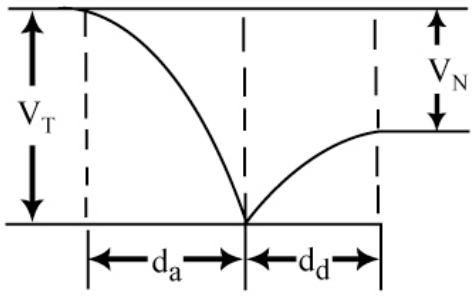

More specifically, it can be shown that Eq. (6) still controls the current provided that,

$$\frac{d_d}{d_a} > \left(1-\sqrt{R}\right)^{1/2}\left(1+2\sqrt{R}\right) \qquad \text{with} \qquad R \;=\; \frac{V_N}{V_T} \tag{11}$$

(for equal gaps, this is satisfied for all R between 0 and 0.75. For instance, at higher R, the second gap limits current). Accepting, then, Eq. (6), the thrust is again given by $\dfrac{F}{A} = \dfrac{\dot{m}}{A}c$, where $\dfrac{\dot{m}}{A}$ has not changed, but c is proportional to $V_N^{1/2}$. Hence we obtain, instead of Eq. (9),

$$\frac{F}{A} \;=\; \frac{8}{9}\varepsilon_0\frac{V_T^{3/2}V_N^{1/2}}{d_a^2} \;=\; \frac{8}{9}\varepsilon_0\left(\frac{V_T}{d_a}\right)^2 R^{1/2} \;=\; \frac{8}{9}\varepsilon_0\left(\frac{V_N}{d_a}\right)^2 R^{-3/2} \tag{12}$$

The last form shows that for a given specific impulse (hence given V_N), reducing $R = V_N/V_T$ increases thrust. It does so by extracting a higher ion current through the flux-limiting first gap.

Returning to Eq. (6), if we imagine a beam with diameter D, we would predict a total beam current of,

$$I_B \;=\; \frac{\pi}{9}\varepsilon_0\sqrt{2\frac{e}{m_i}}\left(\frac{D}{d}\right)^2 V_T^{3/2} \;=\; PV_T^{3/2} \tag{13}$$

where P is the so-called "perveance" of the extraction system. Eq. (13) shows that this perveance should scale as the dimensionless ratio $(D/d)^2$, so that, for example the same current can be extracted through two systems, one of which is twice the size of the other, provided diameter and grid spacing are kept in the same ratio.

While the one-dimensional model is important in identifying many of the governing effects and parameters, its quantitative predictive value is limited. Three-dimensional effects, such as those of the ratio of extractor to accelerator diameter, the finite grid thicknesses, the potential variation across the beam etc. are all left out of account. So are also the effects of varying the properties of the upstream plasma, such as its sheath thickness, which will vary depending on the intensity of the ionization discharge, for example.

Also, for small values of $R = V_N/V_T$, the beam potential (averaged in its cross-section) cannot be expected to approach the deep negative value of the accelerator, particularly for the very flattened hole geometry prevalent when d/D is also small. Thus, the perveance per hole can be expected to be of the functional form,

$$P = P\left(\frac{d}{D}, \frac{D_a}{D_s}, \frac{t_a}{D_s}, \frac{t_s}{D_s}, R, \frac{V_D}{D_T}\right) \tag{14}$$

where the subscripts (s) and (a) identify the screen and accelerator respectively, t is the grid thickness, and V_D is the discharge voltage, which in a bombardment ionizer controls the state of the plasma. These dependencies have been examined for a 2-grid extractor in an Argon-fueled bombardment thruster. Some of the salient conclusions will be summarized here:

1. Varying the screen hole diameter D_s while keeping constant all the ratios (d/D_s, D_a/D_s, etc) has only a minor effect, down to $D_s \sim 0.5$ mm if the alignment can be maintained. This confirms the dependence upon the ratio d/D_s.

2. The screen thicknesses are also relatively unimportant in the range studied ($t/D_s \sim 0.2 - 0.4$).

3. Reducing $R = V_N/V_T$ always reduces the perveance, although the effect tends to disappear at large ratios of spacing to diameter (d/D_s), where the effect of the negative accelerator grid has a better chance to be felt by the ions. The value of d/D_s at which R becomes insensitive is greater for the smaller R values.

4. For design purposes, when V_N and not V_T is prescribed, a modified perveance $I_B/V_N^{3/2}$ (called the "current parameter") is more useful. As Eq.(13) shows, one would expect this parameter to scale as $R^{-3/2}$, favoring low values of R (strong accel-decel design). This trend is observed at low R, but, due to the other effects mentioned, it reverses for R near unity, as shown in the figure below.

   This is especially noticeable at small gap/diameter ratios, when a point of maximum extraction develops at $R \sim 0.7 - 0.8$, which can give currents as high as those with $R \sim 0.2$. However, as the figure also also shows, the low R portion of the operating curves will give currents which are independent of the gap/diameter ratio (this is in clear opposition to the 1-D prediction of Eq. (13)). Thus, the current, in this region, is independent of both d and D_s. This opens up a convenient design avenue using low R values: Fix the smallest distance d compatible with good dimensional control, then reduce the diameter D_s to the smallest practicable size (perhaps 0.5 mm). This will allow more holes per unit area (if the hole spacing varies in proportion to their size), hence more current per unit grid area.

5. The perveance generally increases as D_a/D_s increases, with the exception of cases with R near unity, when an intermediate $D_a/D_s = 0.8$ is optimum.

6. Increasing V_D/V_T, which increases the plasma density, appears to flatten the contour of the hole sheath, which reduces the focusing of the beam. This results in direct impingement on the screen, and, in turn, forces a reduction of the beam current.

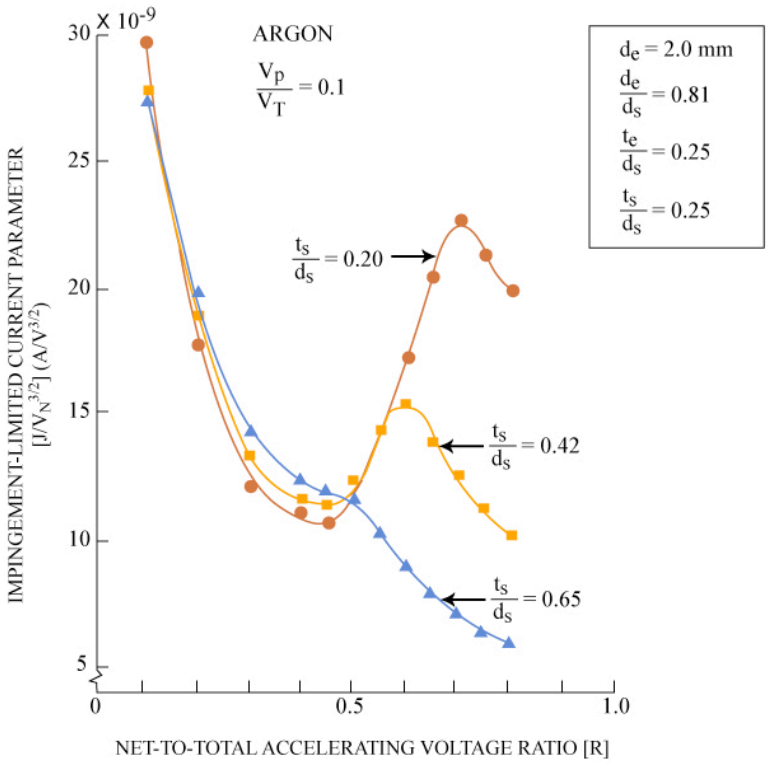

Some appreciation for the degree to which Child-Langmuirs law departs from the observed current extraction capacity of real devices can be obtained from the data for the 30 cm J-series thruster (this is the precursor of the very successful ion engines on the Dawn spacecraft). In this case, we have $d = 0.5$ mm, $t_a = t_s = 0.38$ mm, $D_s = 1.9$ mm, $D_a = 1.14$ mm, and a total of 14860 holes. We will refer to data with Xe, for $R = V_N/V_T = 0.7$ and $V_D = 31.2$ V, $V_N = 1200$ V. The reported beam current in this case is $I_B = 4.06$ A. A correlation for various propellants is,

$$I_B = = \frac{17.5(V_T/1000)^{2.2}}{\xi\sqrt{M}} \pm 25\% \tag{15}$$

where ξ is a double-ion correction factor, given as 0.934 for this case, and M is the molecular mass in *amu*. The power of 2.2 instead of 1.5 for the effect of extraction voltage is to be noticed. This correlation yields for our case $I_B = 5.4$ A, on the outer boundary of the error band.

For these data, if we apply the Child-Langmuir law Eq.(13) to each hole (diameter D_s), and use directly the spacing $d = 0.5$ mm, we obtain a hole current of 3.83 mA, or, in total $I_B = 57.1$ A, i.e., 14 times too high. An approximate 3-D correction is to replace d^2 by $(d + t_s)^2 + D_s^2/4$ in Child-Langmuir's equation. This gives now $I_B = 8.4$ A, still twice the experimental value. In any event, these results show that important departures from 1-D estimates can be expected, so analysis in the design phase should be approached with care.

To complete this discussion, two limiting conditions should be mentioned here:

a) *Direct ion impingement on screen:* At low beam current, the screen collects a very small stray current, which is due to charge-exchange ion-neutral collisions in the accelerating

gap: after one such collision, the newly formed low speed ion is easily accelerated into the screen. The screen current takes, however, a strong upwards swing when the beam current increases beyond some well defined limit. This is due to interception of the beam edges, and, since the high energy ions are very effective sputtering agents, results in a very destructive mode of operation. All the perveance values shown in the figure, for instance, are impingement-limited, i.e., correspond to the highest current prior to onset of direct impingement.

b) *Electron back-streaming:* For R values near unity, the barrier offered by the accelerator negative potential to the neutralizer electrons becomes weak, and beyond some threshold value of R, electrons return up the accelerator potential to the chamber. This results in screen damage, space charge distortion, and shorting of the neutralizer supply. Kaufman gave the theoretical estimate,

$$R_{max} \;=\; 1 - \frac{0.2}{\left(\frac{I_E}{D_A}\right) \exp\left(\frac{t_a}{D_A}\right)} \tag{16}$$

which was confirmed experimentally, except that it was found to be a somewhat conservative estimate.

Physical Process in Electron Bombardment Ionization Chambers

In an electron bombardment ionizer, the neutral gas is partially ionized by an auxiliary dc discharge between conveniently located electrodes. Of these, the anode is the same anode which receives the electrons from the ionization process (see the ion engine diagram). The primary electrons responsible for the ionization of the neutral gas are generated at a separate cathode, which can be a simple heated tungsten filament, or for longer endurance, a hollow cathode. The cathode-anode potential difference V_D is selected in the vicinity of the peak in the ionization cross-section of the propellant gas, which occurs roughly between three and four times the ionization energy (i.e., around 30-50 Volts for most gases). The structure of the potential distribution in the discharge is very unsymmetrical: most of the potential difference V_D occurs in a thin sheath near the cathode, and the body of the plasma is nearly equipotential, at a level slightly above that of the anode (typically the anode current density is below the electron saturation level, and so an electron-retarding voltage drop develops).

Ionization is due both to the nearly mono-energetic primary electrons (with energies of the order of eV_D) and to the thermalized secondary electrons themselves. These have typically temperatures (T_m) of a few eV, so that only the high energy tail of the Maxwellian energy distribution is above the ionization energy and can contribute to the process, but their number density greatly exceeds that of the primaries, and both contributions are, in fact, of the same order. It is therefore desirable to maximize the residence time of both types of electrons in the chamber before they are eventually evacuated by the anode. This is achieved by means of a suitable distribution of confining magnetic fields. The figure below show three types of magnetic configurations, of which only the last two are today of practical importance. The magnetic field strengths can vary from about 10 to 1000 Gauss, depending on type and location.

The ions generated in the active part of the discharge chamber are only weakly affected by the magnetic field, and so they wander at random, colliding rarely with neutral atoms before

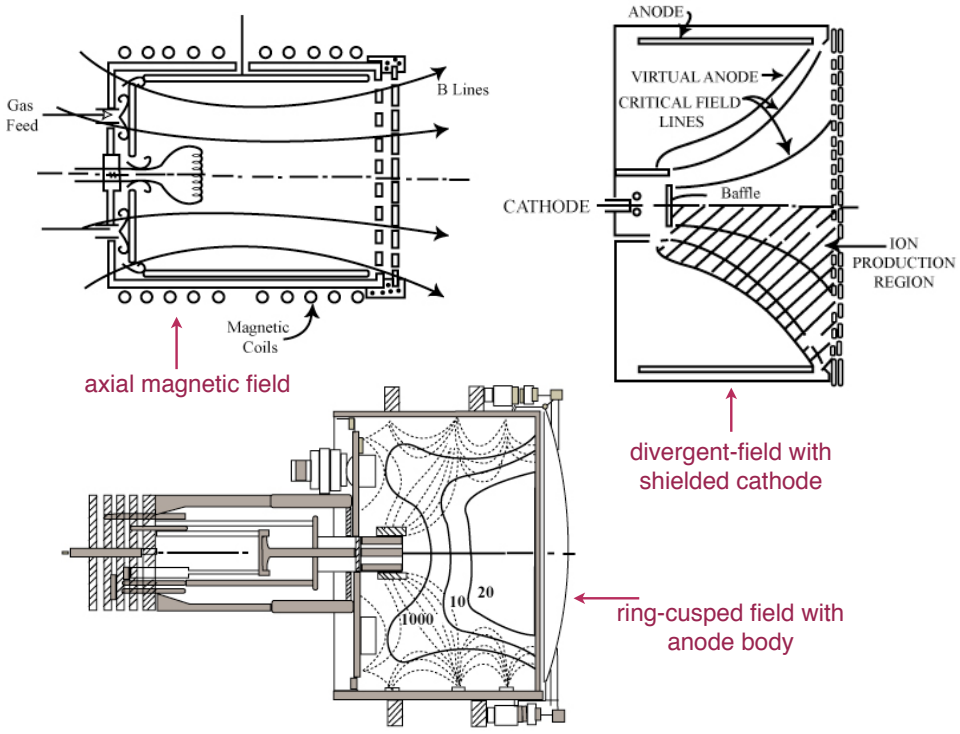

reaching any of the wall surfaces. Since these walls (or the cathode itself) are all negative with respect to the plasma, the ions penetrate the negative sheaths at a velocity of the order of the so-called Bohm velocity, or isothermal ambipolar speed of sound,

$$v_B = \sqrt{\frac{kT_e}{m_i}} \tag{17}$$

and are then further accelerated in the sheath. Those that happen to arrive at one of the extractor hole sheaths become thus the ion beam, but those arriving at solid walls collide with them at an energy corresponding to that of the sheath, which often leads to sputtering, and are neutralized. They then return as neutrals to the plasma, where they are again subject to ionization or excitation processes.

Nature of the Losses

Since electron-ion recombination, even if it did happen in the beam, would contribute nothing to the engine thrust, the ionization energy per beam ion is the minimum energy expenditure required. This would amount to 10.5 eV in Hg, 15.8 in Argon or 12.1 eV in Xenon. In reality the energy loss per beam ion ranges from about 100 to 400 or more eV. The sources of the additional losses can be identified from the description of processes in the previous section:

a) Some primary electrons reach the anode and surrender their high energy.

b) The thermal electrons arrive at the anode with energies of a few eV.

c) Ions that fall to cathode-potential surfaces lose their kinetic energy to them. In addition, they also lose the energy spent in their ionization.

d) Metastable excited atoms surrender the excitation energy upon wall collision.

e) Short-lived excited atoms emit radiation, which is mostly lost directly.

Of a different nature are the energy losses required to heat the cathode emitters or, in the case of Hg, the vaporizers and chamber walls. Finally, not all the injected gas leaves in the form of ions (only a fraction η_u, called the "utilization factor" does). At the best conditions, η_u ranges from 75 to 95%. It is of interest to examine the relationship between η_u and the degree of ionization, α, in the chamber plasma. If n_e is the electron (and ion) density, the flux of ions being extracted is approximately,

$$\Gamma_i \;=\; n_e v_B \phi_s e^{-1/2} \tag{18}$$

where ϕ_s is the open area fraction of the screen grid. For convenience, we lump the $e^{-1/2}$ factor into the definition of ϕ_s. The flux of neutrals through the same overall area is,

$$\Gamma_n \;=\; n_n \frac{\bar{c}_n}{4}\phi \tag{19}$$

where $\bar{c}_n = \sqrt{\dfrac{8kT_e}{\pi m_n}}$ is the mean thermal speed of the heavy particles, and ϕ is an open-area fraction for the combination of grids, reflecting the fact that neutrals, unlike ions, are not focused into the accelerator grid holes, if ϕ_s and ϕ_a are the geometrical open-area fractions of the screen and accelerator grids, we have,

$$\frac{1}{\phi} \;=\; \frac{1}{\phi_s} + \frac{1}{\phi_a} - 1 \tag{20}$$

The ratio of (18) and (19) gives, after rearrangement,

$$\frac{\alpha}{1-\alpha} \;=\; \frac{\phi}{\phi_s\sqrt{2\pi}}\sqrt{\frac{T_n}{T_e}}\frac{\eta_u}{1-\eta_u} \tag{21}$$

where,

$$\alpha = \frac{n_e}{n_e + n_n} \qquad \text{and} \qquad \eta_u = \frac{\Gamma_i}{\Gamma_i + \Gamma_n} \tag{22}$$

As an illustration, using once again the J-series Xenon data, if $\phi_s = 0.67$, $\phi_a = 0.24$ (hence $\phi = 0.215$), and if we take $T_e = 70,000$ K $= 6.03$ eV, $T_n = 400$ K (wall temperature), and $\eta_u = 0.8$ (a common operating point) we obtain $\alpha = 0.0372$, i.e., a 3.7% ion density fraction guarantees an 80% ion flux fraction.

Sheath dimension and implication for screen hole diameter

In many plasma devices, such as ion engines, the electric potential is directly applied between electrodes. The anode will lie at a potential below the plasma potential as determined in Lecture 8, but the cathode surfaces will (including the screen grid) will be forced to a voltage ϕ_D below the anode potential. The general question now is how thick will the sheath region be under this forced potential bias. This has implications to the maximum size of holes in the screen and accelerator grids of ion engines.

To simplify this analysis we assume that under the strong forced bias, the sheath region is space-charge limited. We then use the Child-Langmuir relation to find the ion current density,

$$j_i \;=\; \frac{4}{9}\varepsilon_0\sqrt{2\frac{e}{m_i}}\frac{\phi_D^{3/2}}{\delta^2} \tag{23}$$

which is also equal to $j_i = en_{e_\infty}e^{-1/2}v_B$. Therefore, the sheath size is approximated by,

$$\frac{\delta}{\lambda_D} \;\approx\; \left(\frac{e\phi_D}{kT_e}\right)^{3/4} \tag{24}$$

where $\lambda_D = \sqrt{\dfrac{\varepsilon_0 kT_e}{e^2 n_{e_\infty}}}$ is the Debye length.

For 3 eV electrons and $\phi_D = 50$ V, this means that $\delta/\lambda_D \approx 8.4$. The Debye length is about 24 μm, so the sheath size becomes about $\delta \approx 0.2$ mm thick. In the case of the extraction optics of an ion engine, the applied potentials are closer to 1 kV. In that case $\delta/\lambda_D \approx 78$, and $\delta \approx 2$ mm. In consequence, the screen holes need to be smaller than this value, otherwise the plasma would be able to generate a sheath following the contour of the screen material and will *leak* through the grid holes. However, it is also undesirable to make the holes much smaller than δ because there would be significant ion interception on cathode surfaces (low grid transparency). A tradeoff must be reached to find the optimal configuration.

Particle Production Rates

The Ion production rate per unit volume can be expressed as a sum over the various ionizable excited states, involving rate coefficients for both primary and thermalized electrons. The result is $n_m\nu_i$, where the ionization frequency ν_i is,

$$\nu_i = \sum_{\text{excited states}} n_j \left[\frac{n_p}{n_m}P_j'(E_p) + Q_j'(T_m)\right] \tag{25}$$

Here n_m and n_p are the densities of thermalized (Maxwellian) and primary electrons, respectively, and P_j' and Q_j' are rate coefficients for ionization from the j^{th} state by, respectively, primary and Maxwellian electrons. For overall modeling purposes, it is convenient to define an "ion production current" by,

$$I_p \;=\; en_m\nu_i V_p \tag{26}$$

where V_p is the active ion production volume.

Similar atomic calculations can be made for the production rates of each of the excited states, and also of multiple ions. Both data and theory indicate that the ratio $r = I^{++}/I^{+}$ of the fluxes of double and single ions is a function of only the propellant utilization efficiency η_u for a given propellant. Additional data, for the ring-cusp geometry first introduced by Sovey are given in the next figure, which shows that all noble gases fall nearly on the same curve, with mercury having a higher double-ion fraction.

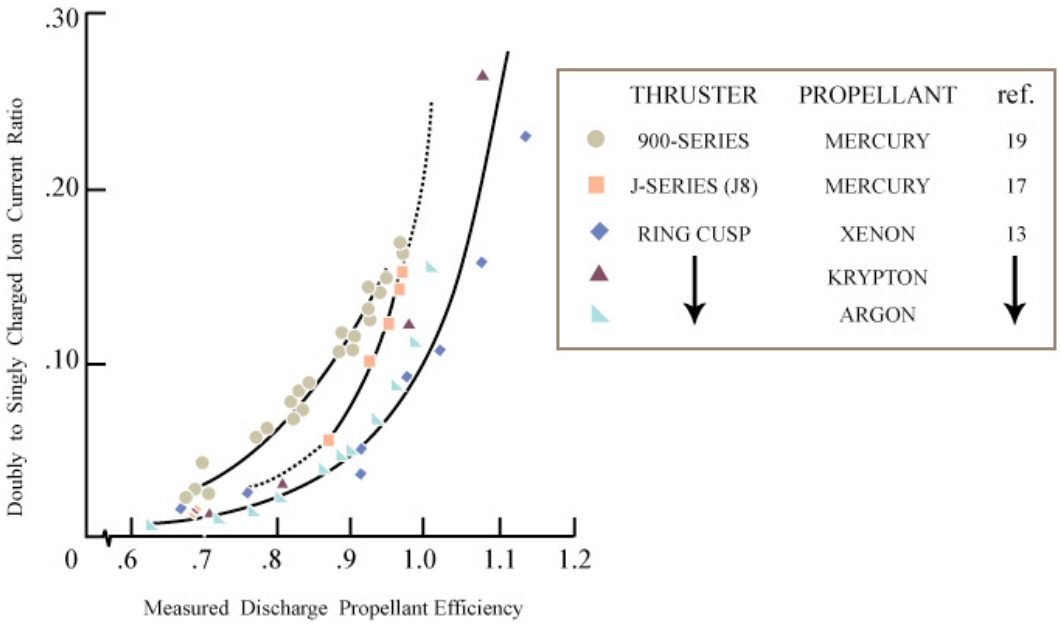

The values of η_u used in the figure are based on the total measured beam current,

$$\eta_u \;=\; \frac{I_B}{I_{tot}} \;=\; \frac{I^+ + I^{++}}{I_{tot}} \qquad \text{with} \qquad I_{tot} \;=\; \dot{m}\frac{e}{m_i} \tag{27}$$

and may exceed unity. The actual flux ratio between charged and uncharged particles is,

$$\eta_u \;=\; \frac{I^+ + \frac{1}{2}I^{++}}{I_{tot}}$$

so that a correction factor should be applied to the current-based utilization factor, given by,

$$\beta \;=\; \frac{1 + r/2}{1 + r} \tag{28}$$

Similarly, the presence of the double ions reduces the thrust by a factor:

$$\psi \;=\; \frac{1 + r/\sqrt{2}}{1 + r} \tag{29}$$

The total ion production rate in the plasma I_p is given by Eq. (26), and an electron current of equal magnitude is also produced, which must be evacuated by the anode. In addition, the anode must also evacuate the electron current I_E emitted by the cathode. The two together make up the "discharge current",

$$I_D \;=\; I_p + I_E \tag{30}$$

The discharge power supply, connected between anode and cathode at a voltage V_D must handle this current I_D, and hence consumes a power $I_D V_D$.

Of the ions produced (I_p) a current I_B is extracted into the beam, while a small current I_{acc} is intercepted by the accelerator grid. The balance is the stray ion current that goes to the cathode-potential surfaces (cathode-screen-casing),

$$I_C \;=\; I_p - I_B - I_{acc} \tag{31}$$

Electrons are returned to the cathode-potential structure by the discharge power supply, at the rate I_D. Electrons are also removed from it by the cathode itself (I_E), by the neutralizer power supply, which must send to the neutralizer an electron current equal to the ion beam current I_B, and, to a small extent, by the accelerator power supply to neutralize the intercepted ion current I_{acc}. Setting the total rate of positive charge gain to zero,

$$(I_p - I_B - I_{acc}) - I_D + I_E + I_B + I_{acc} \;=\; 0 \tag{32}$$

which agrees with Eq. (30).

For design purposes, as well as for characterization of existing engines, it is useful to develop aggregate physical models of the performance of ionization chambers, where temperatures, densities, etc., are either assumed to be constant or are given their average value.

Propellant Selection

As implied by many points of the preceding discussion, the ideal propellant for an ion thruster would have a high molecular mass, low first ionization potential and high maximum cross-section for 1st ionization (but the reverse properties for 2nd and higher levels of ionization), and it should also be easy to store and handle and be benign in terms of materials compatibility and human safety. Mercury has many of these attributes, except for its low 2nd ionization threshold and its toxicity and chemical aggressiveness in general. The same can be said to a greater extent about Cesium, which, because of its handling difficulty, has been only used in contact ionization thrusters. Concerns about spacecraft contamination by condensation of plume-derived atoms on external surfaces has led to a shift away from Hg (and any other liquid metals) and towards alternative, safer propellants. Molecular gases tend to be rejected because of the multiplicity of ionic and excited species their discharges can generate, and thus the noble gases are the natural choice, especially Xenon, which is the heaviest (and easiest to ionize) of the naturally occurring noble gases. Argon has also been considered due to its low cost.

The table below gives a compilation of physical and operational properties of these propellants, with some comments as to their impact on thruster operation. The overall performance with Xe is very similar to that with Hg, although the efficiency at a given thrust level is slightly better in Hg. It has been shown that the efficiency correlates uniquely with the product of the specific impulse, the square root of the molecular mass and the double-ion factor ψ, although this depends to some extent upon the choice of other parameters. Thus, the simplified performance modeling based upon the "loss velocity" appears justified.

	SPECIES			
PROPERTY	Hg	A	Xe	IMPACT
1st ionization potential (eV)	10.43	15.8	12.13	Hg best, lower ionization losses
2nd ionization potential (eV)	29.2	27.6	33.3	Higher 2nd leads to fewer 2nd ions
3rd ionization potential (eV)	63.4	45	65.5	High enough in all
1st excitation potential (eV)	4.8	11.7	8.39	More radiation from Hg
2nd excitation potential (eV)	4.6 (Metast.)	13.2	8.28 (Metast.)	More effective Hollow Cathodes in Hg
3rd excitation potential (eV)	5.4 (Metast.)	14.1	9.4 (Metast.)	More effective Hollow Cathodes in Hg
Atomic Mass (AmU)	200.59	39.9	131.3	Lowest acceleration voltage for an Isp in Hg. Lowest current for a given thrust in Hg.
Boiling Point (°C)	356.58	-189.2	-107 +/- 3	Only Hg storable as liquid
Storage Condition	Liquid $\rho = 13.6$ g/cm^3	Compr. Gas or Cryogenic Liq.	Near Critical $\rho = 0.5$ g/cm^3 at 35 °c, 60 Bar	Hg and Xe both compact tanks. A bulkier.
Chemical Activity (Toxicity)	High	None		A, Xe safer. Cu, Al, common brazes can be used.
Cost	Moderate	Low	High	May be issue in large systems
(Relative) Sputtering yield	1	4	2	Higher erosion in A, Xe, despite fewer 2nd ions.
Propellant Flow Control	Simple, through vaporizer T-cont.	More Complex through plenum, control or servo-needle valve		Heavier propellant system in A, Xe (despite elimination of heaters)
Power Processing		No need for heaters on fuel lines, vaporizer		Higher reliability with A, Xe. Also, some loss reductions.